Unsymmetric vesicles with a different design on each side for near-infrared fluorescence imaging of tumor tissues†

Akihiro Uesaka,[a] Isao Hara,[b] Tomoya Imai,[c] Junji Sugiyama[c] and Shunsaku Kimura*[a]

Spherical vesicular assemblies with unsymmetric membranes are prepared from A_3B-type and AB'-type peptides with different helix senses in the hydrophobic B and B′ blocks under the control of three associated factors: stereo-complex formation, dipole–dipole interactions, and steric effects. $[(Sar)_{26}]_3$-*b*-(L-Leu-Aib)$_6$ (**A_3BL**), $(Sar)_{27}$-*b*-(L-Leu-Aib)$_6$ (**ABL**), $(Sar)_{28}$-*b*-(D-Leu-Aib)$_6$ (**ABD**), lipoic-acid terminated **ABL** (**lipoABL**), and lipoic-acid terminated **ABD** (**lipoABD**) are mixed while keeping equimolar ratios of the total amounts of the right- and the left-handed helices. When **A_3BL** exceeds more than 60% of all the right-handed helices of the mixture, the unsymmetric vesicles are formed, as indicated by the selective adsorption of gold nanoparticles on the vesicle surface observed by TEM. The unsymmetric vesicles are also prepared using **ICGABL** and **ICGABD** with a near-infrared fluorophore, indocyanine green (ICG), at the terminals of **ABL** and **ABD**. The unsymmetric vesicle formation is verified by fluorescence quenching with the addition of In ions to the solution. When these vesicles are injected into tumor-bearing mice, the vesicles are effectively accumulated into tumor tissues *via* the EPR effect. The unsymmetric vesicle containing ICG at the inward surface induces less IgM production than that with ICG at the outward surface. More stealth vesicles in the blood stream are therefore obtainable by concealing the imaging fluorophores in the vesicle.

1. Introduction

Amphiphilic molecules self-assemble into molecular assemblies in water *via* various intermolecular interactions such as hydrophobic and electrostatic interactions.[1–5] Their morphologies depend heavily on the chemical structure of the components, and suitable molecular designs have been proposed to generate molecular assemblies with various morphologies and sizes.[6–8] In addition, molecular assemblies have been applied for broad fields ranging from nanodevices to biomaterials.[9–14]

Among them, vesicles are one of the most frequently appearing nanocarriers for tumor-targeted drug delivery and molecular imaging.[15–20] In tumor tissues, the vascular walls have submicron holes because of rapid angiogenesis; therefore, nanocarriers can permeate into tumors through the vascular wall. Furthermore, the lymph system around tumors grows so slowly that nanocarriers are usually retained in the tumor. This

[a]Department of Material Chemistry, Graduate School of Engineering, Kyoto University, Kyoto-Daigaku-Katsura, Nishikyo-ku, Kyoto, 615-8510, Japan. E-mail: shun@scl. kyoto-u.ac.jp; Fax: +81-75-383-2401; Tel: +81-75-383-2400

[b]Technology Research Laboratory, Shimadzu Corporation, 3-9-4 Hikari-dai, Seika-cho, Soraku-gun, Kyoto 619-0237, Japan

[c]Research Institute for Sustainable Humanosphere (RISH), Kyoto University, Gokasho, Uji, Kyoto 611-0011, Japan

† Electronic supplementary information (ESI) available. See DOI: 10.1039/c4ra15635h
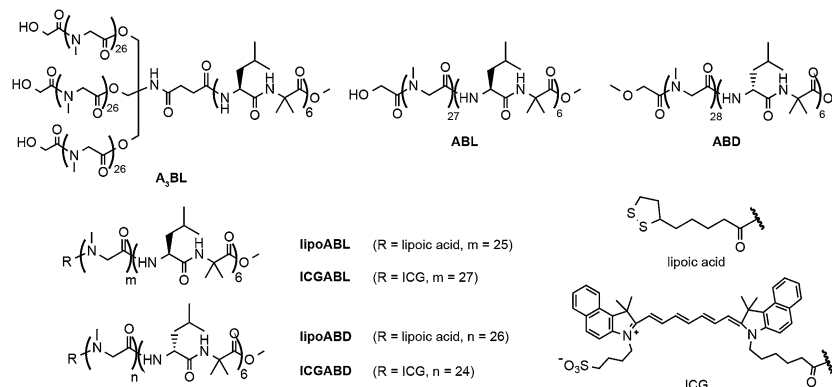
effect is called the enhanced permeability and retention (EPR) effect.[21] In this regard, the control of the nanocarrier size is essential to allow them to be passively accumulated into tumor tissues.[18,22,23] Various vesicles of liposomes, polymersomes, and peptosomes, which are prepared from lipids,[24,25] polymers,[26,27] and peptides,[18,28] respectively, have been studied. One challenge of vesicular molecular assemblies is to prepare unsymmetric vesicles with different components between the outer and the inner surfaces that mimic cell membranes. For example, Fuhrhop reported that unsymmetric bolaamphiphiles with small and large head groups self-assemble into unsymmetric monolayer vesicles *via* steric effects.[29,30] Furthermore, Xiao and Pautot reported that reverse micelles were transformed into lipid monolayers at the oil/water interface to form unsymmetric vesicles.[31,32] However, it is not so easy to prepare unsymmetric membranes under precise control of the distribution of the components. In addition, these methods do not seem to be applicable to the unsymmetric self-assembly of amphiphilic polymers due to the disordered packing and/or molecular entanglement of the hydrophobic blocks.

We previously reported that left-handed helical peptides with one hydrophilic chain (AB-type) and right-handed helical peptides with three hydrophilic chains (A_3B'-type) co-assemble into unsymmetric peptosomes *via* stereo-complex formation, dipole–dipole interactions, and steric effects.[33] Stereo-complex formation and dipole–dipole interactions can result in

Fig. 1 Chemical structures of amphiphilic block polypeptides **A₃BL**, **ABL**, **ABD**, **lipoABL**, **lipoABD**, **ICGABL**, and **ICGABD**.

regularly interdigitated helix packing to generate unsymmetric planar sheets. The planar sheets grew into unsymmetric vesicles due to the steric effect of the bulky hydrophilic A_3 moieties of the A_3B-type peptides extruding to the outer surface. Furthermore, the selective surface modification at the outer or inner surface can be easily performed by choosing the right-handed or left-handed helix of the functionalised helical peptides.

In this paper, we study a necessary proportion of the A_3B-type helix, $[(Sar)_{26}]_3\text{-}b\text{-}(\text{L-Leu-Aib})_6$ (**A₃BL**), for the generation of unsymmetric vesicles in mixtures of the A_3B-type right-handed helical peptide (**A₃BL**), AB-type right-handed helical peptide, $(Sar)_{27}\text{-}b\text{-}(\text{L-Leu-Aib})_6$ (**ABL**), AB-type left-handed helical peptide, $(Sar)_{28}\text{-}b\text{-}(\text{D-Leu-Aib})_6$ (**ABD**), and two AB-type helical peptides with lipoic acid at the termini of the hydrophilic chains, **lipoABL** and **lipoABD** (Fig. 1). Lipoic acid at the terminal of the poly(sarcosine) chain has been shown to behave as a hydrophilic group in these molecular assemblies.[33,34] Unsymmetric vesicles about the location of near-infrared fluorescent (NIRF) probe are also prepared here using the novel functional AB-type helical peptides modified with indocyanine green (ICG), **ICGABL** and **ICGABD** (Fig. 1). Using these two types of unsymmetric vesicles, one with ICG groups on the outer surface and the other with ICG groups on the inner surface, we examine the *in vivo* distributions of these vesicles and the IgM productions in tumor-bearing mice to obtain information of the effect of surface modification on the pharmacokinetics of the vesicles.

2. Experimental section

2.1 Materials

The amphiphilic peptides **A₃BL**, **ABL**, **ABD**, **lipoABL** and **lipoABD** were obtained as reported previously.[33,34] **ICGABL** and **ICGABD** were synthesised according to Scheme S1 (ESI†). The synthetic details are described in the ESI.† The near-infrared fluorescence compound, ICG-sulfo-OSu, was purchased from Dojin Laboratory Ltd. Au nanoparticles (AuNPs) were purchased from BB international (U.K.) with an average diameter of 10 nm. All reagents were purchased commercially and used as received unless otherwise noted.

2.2 Preparation of molecular assembly

A solution of polypeptides in ethanol (0.05 mg μL⁻¹, 5.0 μL) was injected into milliQ water under stirring at 4 °C. In the case of **A₃BL**, methanol was used instead of ethanol. After 30 min, the dispersion was heated by an aluminium heat source if necessary, followed by cooling at room temperature for measurements.

2.3 Transmission Electron Microscopy (TEM)

TEM images were collected using a JEOL JEM-2000EXII at an accelerating voltage of 100 kV. Peptide aqueous solutions were applied on a carbon-coated Cu grid, and the samples were negatively stained with 2% uranyl acetate followed by suction of the excess fluid with a filter paper.

2.4 Frozen-hydrated/cryogenic-TEM (Cryo-TEM)

The peptide dispersions were quickly frozen in liquid ethane, which was cooled with liquid nitrogen. The samples were examined at an accelerating voltage of 100 kV at the temperature of liquid nitrogen.

2.5 Dynamic Light Scattering (DLS)

The DLS measurements were taken using a DLS-8000KS (Photal Otsuka Electronics) with a He–Ne laser at 25 °C. Before the DLS measurements, each prepared sample was filtered using a 0.20 μm PVDF (polyvinylidene fluoride) syringe filter (GE Healthcare UK limited).

2.6 The adhesion of AuNPs to vesicles

Preliminarily, peptides with lipoic acid were mixed with the solution of amphiphilic peptides, and the molecular assemblies were prepared from the solutions according to the previously described procedure.[33] The peptide aqueous solutions were applied on a carbon-coated Cu grid, and AuNPs with diameters of 10 nm were then added on the grid to reduce the non-specific association of AuNPs with vesicles. The lipoic acids on the molecular assemblies can easily react with AuNPs on the Cu grid.[33,34] After washing the excess AuNPs with dispersion media,

the samples were negatively stained with 2% uranyl acetate followed by suction of the excess fluid with a filter paper.

2.7 Fluorescent analysis

The fluorescent spectra of the peptide dispersions were obtained using a JASCO FP-6600 spectrofluorometer at an optional temperature with a transmission cell with an optical path length of 1 cm. Before measurements, vesicle suspensions were diluted to 0.05 mg mL^{-1} (in a total volume of 2.0 mL). The excitation wavelength of ICG is 755 nm.

2.8 *In vivo* NIRF-imaging of vesicles with ICG

SUIT2/pEF/LUC cells (5×10^5 cells) were dissolved in PBS (20 μL) and subcutaneously inoculated into the right femoral region of seven-week-old BALB/c nu/nu mice ($n = 3$ per group). Vesicles containing ICG were prepared in milliQ water, and NaCl was added into the suspensions to adjust to physiological conditions (0.9 wt% NaCl aq.). The vesicle suspensions (5 mg kg^{-1}, 100 μL) were injected into the mice *via* the tail vein one week after the tumor transplantation. The amount of injected ICG was 10 nmol kg^{-1}. NIRF images (Ex, 785 nm; Em, 845 nm) were taken at 15 min, 1 h, 3 h, 6 h, 9 h, and 24 h after the dose. During the imaging process, the mice were held on the imaging stage under anesthetised conditions with 2.5% of isoflurane gas in air flow (1.5 L min^{-1}). The pseudo images were constructed from the photon counts.

2.9 IgM assay

For ELISA, vesicles (5 mg kg^{-1}, 100 μL) were injected to the BALB/c nu/nu mice, which were purchased from Japan SLC, Inc. (Japan; $n = 3$ per group). Mouse blood was collected in 1.5 mL tubes from the inferior vena cava under anaesthesia conditions at one week after administration. The serum was kept overnight at 4 °C. The next day, the serum was obtained by centrifugation (10 min, 3000 rpm) and saved at −40 °C.

Lactosomes prepared from [poly(Sar)$_{50}$]$_3$-*b*-poly(L-lactic acid)$_{30}$ in 50 μL acetonitrile were added to 96-well plates (0.5 μg per well) and air dried completely for one day. Then, 150 μL of blocking buffer [2% BSA/phosphate-buffered saline (PBS)] was added and incubated for 2 h. The wells were washed four times with washing buffer (PBS-T: 0.05% tween 20 in PBS). The serially diluted sera were added to the wells and incubated for 2 h. After incubation, the wells were washed four times with PBS-T. Peroxidase-conjugated goat-anti-mouse IgM in 0.1% BSA/PBS (50 μL, Southern Biotech, USA) was added as the secondary antibody. After the solution was incubated for 2 h, the wells were again washed four times with PBS-T. *o*-Phenylenediamine (0.5 mg mL^{-1}, Sigma, St Louis, MO) dissolved in 0.0003% H$_2$O$_2$-0.1 M citrate phosphate buffer (pH 5.0) was added to the wells. At 10 min after the *o*-phenylenediamine addition, the OD was determined at 490 nm with 620 nm as a reference.

2.10 Statistical analysis

All results are expressed as mean ± SD. Differences between groups in amount of AuNPs attached on vesicles, IgM

production and NIRF-imaging studies were assessed by the *t*-test for independent samples. *P*-values <0.05 and <0.01 were considered statistically significant and designated by * and **, respectively.

2.11 Ethics

All of our *in vivo* animal experiments were approved by the animal research committee of Kyoto University. The animals were treated humanely.

3. Results and discussions

3.1 Preparation of unsymmetric vesicles

A$_3$BL and **ABD** were co-assembled into planar sheets with lengths of *ca.* 150 nm in milliQ water (Fig. 2a), and these sheets were transformed into vesicles with diameters of *ca.* 90 nm upon heating at 90 °C for 1 h (Fig. 2b). DLS measurements showed that the vesicle diameter was 99.6 nm with a narrow size distribution (PDI = 0.052). These results suggest that the stereocomplex formation contributes to the formation of the planar sheet morphology, and the subsequent heat treatment triggers vesicle formation so as to reduce the hydrophobic edges in water, as reported previously.[33–35]

To study the unsymmetry of the vesicle, **lipoABL** and **lipoABD**, which can bind AuNPs, were incorporated into the vesicles prepared from **A$_3$BL** and **ABD**, respectively.[33] In a previous paper, we demonstrated that lipoic acid at the hydrophilic chain terminal behaves as a hydrophilic moiety.[33,34] If the lipoic acids of amphiphilic peptides are oriented towards the inside of vesicles, AuNPs should not adhere to the vesicles, which can be visualised by TEM to provide information on the peptide orientation in the membrane. AuNPs adhered clearly to the vesicles prepared from **A$_3$BL** + **ABD** + **lipoABL** (0.4/0.5/0.1, mol/mol/mol; Fig. 3a and S2a of ESI†), whereas few AuNPs adhered to the vesicles prepared from **A$_3$BL** + **ABD** + **lipoABD** (0.5/0.4/0.1, mol/mol/mol; Fig. 3b and S2b of ESI†). The TEM images show the collapsed vesicles due to the vacuum condition of the TEM observation, but the morphology was confirmed to be spherical by cryo-TEM observation (Fig. 5). These results indicate that the unsymmetric vesicles were formed from the ternary mixtures, and the functionalised peptides with lipoic acid were integrated into the membrane under control of the molecular orientation according to the right- or left-handed helical sense of the functionalised peptides.
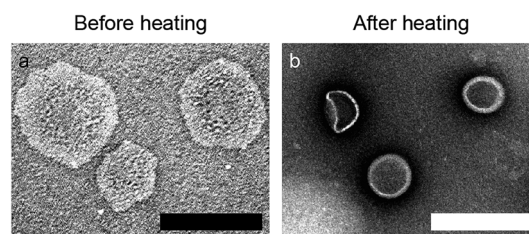

Fig. 2 TEM images (negative stain with 2% uranyl acetate) of molecular assemblies prepared from A$_3$BL and ABD in milliQ water (a) before and (b) after heat treatment at 90 °C for 1 h. Scale bars are 200 nm.
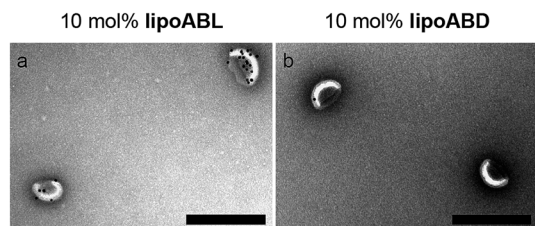
10 mol% **lipoABL**   10 mol% **lipoABD**

Fig. 3 TEM images (negative stain with 2% uranyl acetate) of vesicles prepared from (a) A_3BL + ABD + lipoABL and (b) A_3BL + ABD + lipoABD in milliQ water upon heat treatment at 90 °C for 1 h. An aliquot of a 10 nm AuNP suspension was added to the vesicles on the TEM grid. Scale bars are 200 nm.

3.2 The effect of A_3BL proportion on unsymmetric membranes

To evaluate the proportion of **A_3BL** in all the right-handed helices necessary to achieve the unsymmetric vesicles by steric effects, the compositions of **ABL** and **A_3BL** were varied (Fig. 4). As described above, several AuNPs adhered to the vesicles of **A_3BL** + **ABD** + **lipoABL** (0.4/0.5/0.1, mol/mol/mol), but few AuNPs adhered to those of **A_3BL** + **ABD** + **lipoABD** (0.5/0.4/0.1, mol/mol/mol). The extent of the latter AuNP adherence was similar to that to the vesicles without the lipoic acid-modified peptides (Fig. S3e of ESI†), suggesting the nonspecific adherence of AuNPs in these cases. The quaternary mixture vesicle of **A_3BL**, **ABL**, **ABD**, and **lipoABL** (0.30/0.10/0.50/0.10, vesicle c in Fig. 4), which corresponds to a 60% proportion of the A_3B-type peptide in all the right-handed helices, clearly attached to AuNPs (Fig. S3a of ESI†). On the other hand, when **lipoABL** was replaced by **lipoABD** with the same 60% proportion of the A_3B-type peptide in all the right-handed helices, the quaternary mixture vesicle of **A_3BL**, **ABL**, **ABD**,

and **lipoABD** (0.30/0.20/0.40/0.10, vesicle d in Fig. 4) attached to significantly fewer AuNPs (Fig. S3b of ESI†). It is therefore indicated that the orientation of the peptides should be maintained in the unsymmetric way even in the vesicles containing a 60% proportion of the A_3B-type peptide. The numbers of AuNPs adhered per unit surface area of the vesicles in the TEM images were counted, and the data were analysed statistically (Fig. 4). The selective adherence of AuNPs to vesicles a, b, c, and d was confirmed statistically by a p-value of less than 0.01. It is therefore concluded that all the right-handed helices in these vesicles should orient towards the outside of the vesicle.

However, when the proportion of the A_3B-type peptide decreased to 50% in all the right-handed helices (vesicles e and f in Fig. 4), the extent of AuNP adherence was similar between these vesicles (Fig. S3c and d of ESI†). These results suggest that the molecular direction of helices in the membrane cannot be controlled when the vesicles contain less than 50% A_3B-type peptide in all the right-handed helices.

The DLS measurements revealed that the vesicle diameter increased by increasing the proportion of **ABL** or, in other words, by decreasing the proportion of **A_3BL** (Fig. S4 of ESI†). This result suggests that substituting AB-type peptides for bulky A_3B-type peptides decreases the curvature of the vesicles. Furthermore, the diameter increases sharply when the proportion of **ABL** in all the right-handed helices is more than 50%. This increase also supports the interpretation that bulky A_3B-type peptides start to orient towards the inside of some vesicles when the proportion of **ABL** is more than 50%. From these results, it is concluded that unsymmetric vesicles can be prepared in the presence of A_3BL at a proportion of greater than 60% in all the right-handed helices, and the functionalised unsymmetric vesicles are applicable for some applications that require unsymmetric membranes.
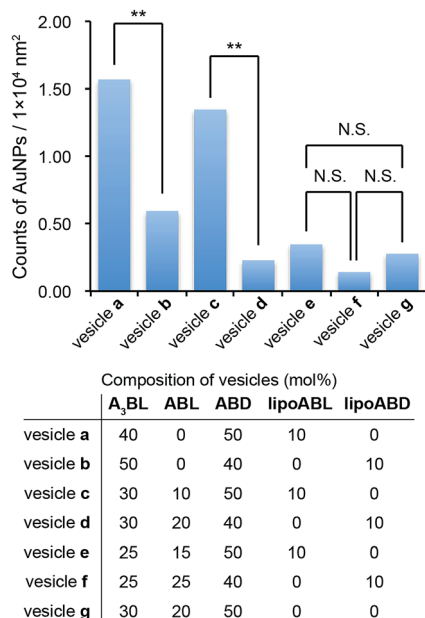
3.3 The application of unsymmetrical vesicles to NIRF imaging

The unsymmetric vesicles were examined as nanocarriers for the NIRF imaging of solid tumor. The ternary mixtures of **A_3BL** + **ABD** + **ICGABL** (0.48/0.5/0.02, mol/mol/mol) and **A_3BL** + **ABD** + **ICGABD** (0.5/0.48/0.02, mol/mol/mol) were self-assembled into homogeneous vesicles in milliQ water (Fig. 5 and S5 of ESI†); the corresponding vesicle diameters determined by DLS were 111.7 nm and 111.5 nm, respectively, which are in agreement with the previously described unsymmetric vesicles. The cryo-TEM images confirm the formation of vesicles, even in the presence of ICG-peptides in these compositions (Fig. 5).

To confirm that vesicles containing ICG also have unsymmetric membranes, aqueous $InCl_3$ was added to the vesicle suspension as a quencher because the hydrophilic poly-(sarcosine) chains of vesicles have been suggested to adsorb In^{3+} ions to effectively quench ICG fluorescence via the heavy-atom effect. When 10 μM aqueous $InCl_3$ was added to vesicles containing ICG-peptides, In^{3+} ions more effectively quenched the fluorescence from the vesicle containing **ICGABL** than from

Fig. 4 The number of AuNPs per unit area (100×100 nm^2) of vesicle surface. The p-value: **p < 0.01.

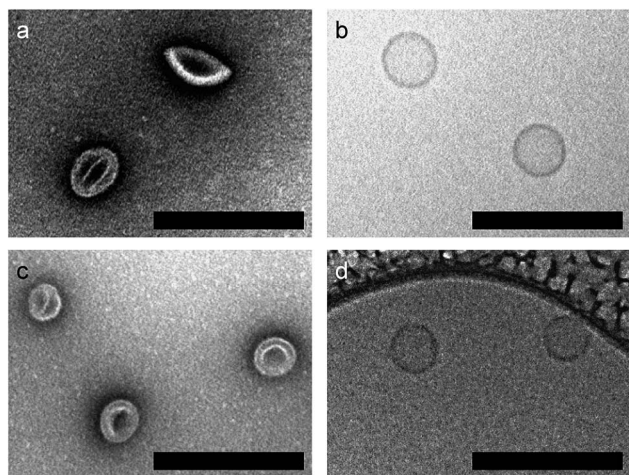| Composition of vesicles (mol%)	A_3BL	ABL	ABD	lipoABL	lipoABD
vesicle a	40	0	50	10	0
vesicle b	50	0	40	0	10
vesicle c	30	10	50	10	0
vesicle d	30	20	40	0	10
vesicle e	25	15	50	10	0
vesicle f	25	25	40	0	10
vesicle g	30	20	50	0	0

Fig. 5 TEM images (negative stain with 2% uranyl acetate) of vesicles prepared from (a) A$_3$BL + ABD + ICGABL and (c) A$_3$BL + ABD + ICGABD in milliQ water upon heat treatment at 90 °C for 1 h. Cryo-TEM images of vesicles prepared from (b) A$_3$BL + ABD + ICGABL and (d) A$_3$BL + ABD + ICGABD. Scale bars are 200 nm.
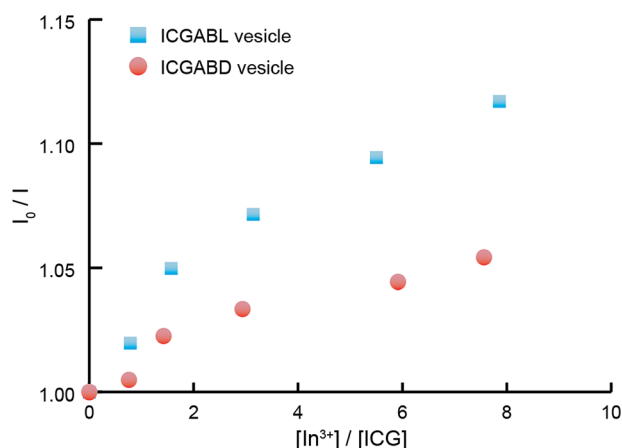

Fig. 6 Stern–Volmer plots of the fluorescence quenching of vesicles containing ICGABL (blue squares) and ICGABD (red circles) by In^{3+} ions.

those containing **ICGABD** according to the Stern–Volmer plots (Fig. 6). The molecular orientation of **ICGABL** and **ICGABD** in each vesicle is therefore controlled to locate at the outside and inside of the vesicles, respectively. In these ternary mixtures, the **A$_3$BL** proportions in all the right-handed helix peptides exceed 96%, and the unsymmetric vesicle formation from these ternary mixtures is consistent with our interpretation of the relationship between unsymmetry and composition.

The *in vivo* dispositions of vesicles containing **ICGABL** and **ICGABD** in tumor-bearing mice were analysed by NIRF imaging (Fig. 7 and S6 of ESI†). These vesicles were prepared in milliQ water, and the concentration of NaCl was adjusted to the physiological condition (0.9 wt%) by the addition of NaCl. The hydrodynamic diameters of both vesicles before and after the salt addition were 112.8 nm (PDI of 0.080) and 109.0 nm (PDI of 0.083), respectively. The integrity of the vesicle with the

added NaCl was also confirmed by cryo-TEM of the unsymmetric vesicle prepared from **A$_3$BL** + **ABD**; the membrane maintained its impermeable property against FITC-dextran incorporated into the vesicle upon the change of ionic strength.[33]

The accumulated amounts of the vesicles in tumor in the right femoral region and in the healthy part of the left femoral region were estimated from the fluorescence intensities of the images. Fig. 7 shows that the vesicle containing **ICGABD** was accumulated more in the tumor than the vesicle containing **ICGABL**. Furthermore, the NIRF images obtained at 5 min after injection show that the vesicle containing **ICGABD** spread over the entire body to fluoresce more intensely than the vesicle containing **ICGABL** (Fig. 7b). The vesicle concentration in the blood stream at 5 min after injection should be therefore be higher for the vesicle containing **ICGABD** than for that containing **ICGABL**. At the moment, the clearance time of the vesicle could not be obtained due to significant capture by the liver; however, these observations support that the vesicle containing **ICGABD** should remain in the blood stream longer than the vesicle containing **ICGABL**, which induced the greater accumulation of the former vesicle in tumors compared to the latter. In the case of the vesicle containing **ICGABD**, the fluorophores were concealed in the unsymmetric vesicle, which should diminish capture by the liver, especially for the ICG fluorophore.

Some nanoparticles have been reported to trigger IgM production when they are dosed to mice.[36–38] For example, polymeric micelles prepared from poly(Sar)$_{64}$-*b*-poly(L-lactic acid)$_{30}$ induced the production of anti-poly(sarcosine) IgM and IgG with a long memory. The amounts of anti-poly(sarcosine) IgM produced by the current vesicles were analysed by ELISA using Lactosome as the positive control (Fig. 8). The vesicles containing ICG-peptides triggered the production of IgM but in less amounts compared with Lactosome. Ishida *et al.* pointed out that the surface density influences the amount of IgM production.[38] On the other hand, we have reported that the high surface density of the poly(sarcosine) chains of nanoparticles suppresses IgM production.[39] In the present case, the A$_3$B-type peptide extruded the bulky A$_3$ moieties outside, and the helical blocks were tightly packed due to stereo-complex formation. The surface density of poly(sarcosine) should therefore be higher with the current vesicles compared to with Lactosome. This higher surface density might explain the ability of the current vesicles to suppress IgM production even though the vesicles have larger diameters (about 100 nm) compared to Lactosome (35 nm).

The vesicle containing **ICGABL** triggered IgM production more than the vesicle containing **ICGABL**. Since the ICG moieties of the vesicle containing **ICGABL** are exposed to the outside of the vesicle, the surface may have more defects than the vesicle containing **ICGABD**, making recognition by B cells easier. It is considered that the unsymmetric vesicles also have different stimulation properties to the immune system.
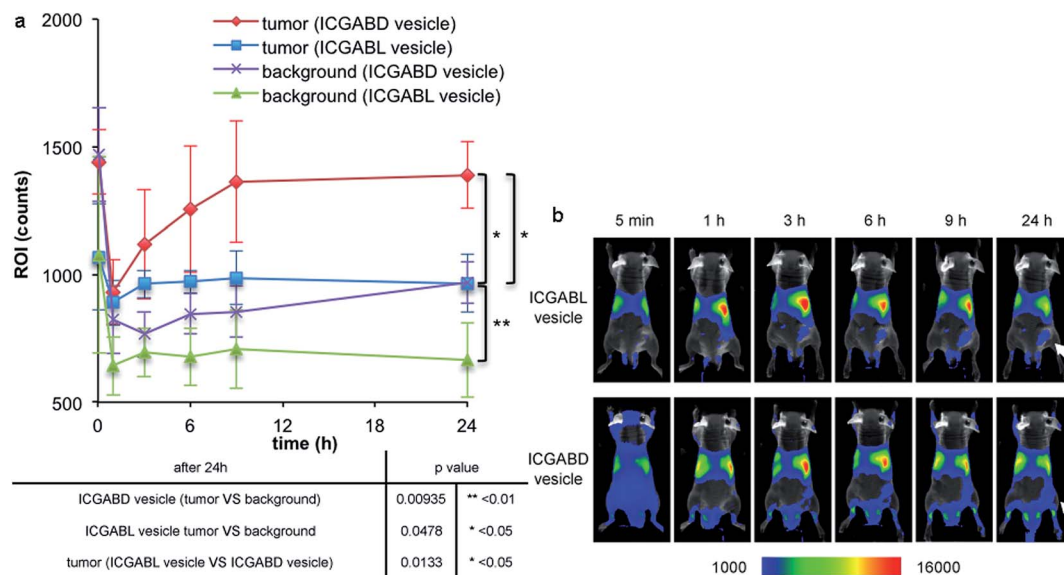
Fig. 7 Accumulations of the vesicles containing **ICGABL** and **ICGABD** in tumor–bearing mice by NIRF imaging ($n = 3$). NIRF images were taken at 15 min, 1 h, 3 h, 6 h, 9 h and 24 h after administration. (a) The vertical axis represents ROI at tumor and background. The p-value: *$p < 0.05$, **$p < 0.01$ (time point is 24 h). (b) *In vivo* NIRF images taken at 24 h after administration. A Clairvivo OPT system was used for the NIRF imaging.
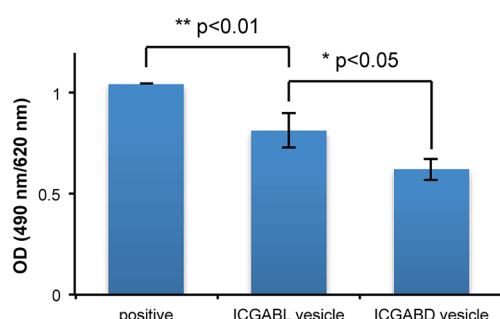

Fig. 8 The production of anti–poly(sarcosine) IgM evaluated by ELISA using a Lactosome plate. The serum was taken at seven days after the dose of Lactosome (positive), the vesicles containing **ICGABL** (ICGABL vesicle), or the vesicles containing **ICGABD** (ICGABD vesicle). The p-value: *$p < 0.05$, **$p < 0.01$.

4.   Conclusions

Unsymmetric vesicles were prepared from mixtures of A_3B-type right-handed helices and AB-type left-handed helices in milliQ water utilising stereo-complex formation, dipole–dipole interactions and steric effects. More than 60% A_3B-type peptides in all the right-handed helices is necessary to obtain unsymmetric vesicles as a result of steric effects. In other words, the vesicles can possibly contain up to 40% functionalised AB-type right-handed helix peptide in all the right-handed helices where all the functional groups are exposed to the outside of the vesicle. Furthermore, the functional groups can be concealed in the inner surface of the vesicle by using a functionalised AB-type left-handed helix peptide. As shown in the present paper, the vesicles show different behaviours regarding *in vivo* disposition and reaction with the immune system depending on the locations of the function groups on the vesicle. We are currently

trying to increase the vesicle accumulation amount in tumors and develop a bimodal imaging vesicle with the unsymmetric vesicle.

Acknowledgements

Notes and references

1 A. D. Bangham and R. W. Horne, *J. Mol. Biol.*, 1964, **8**, 660–668.

2 B. M. Discher, Y.-Y. Won, D. S. Ege, J. C.-M. Lee, F. S. Bates, D. E. Discher and D. A. Hammer, *Science*, 1999, **284**, 1143–1146.

3 D. E. Discher and A. Eisenberg, *Science*, 2002, **297**, 967–973.

4 T. Koga, K. Taguchi, Y. Kobuke, T. Kinoshita and M. Higuchi, *Chem.–Eur. J.*, 2003, **9**, 1146–1156.

5 Z. Liu, J. Qiao, Y. Tian, M. Wu, Z. Niu and Y. Huang, *Langmuir*, 2014, **30**, 8938–8944.

6 J. N. Israelachvili, D. J. Mitchell and B. W. Ninham, *J. Chem. Soc., Faraday Trans. 2*, 1976, **72**, 1525–1568.

7 J. C. M. van Hest, D. a. P. Delnoye, M. W. P. L. Baars, M. H. P. van Genderen and E. W. Meijer, *Science*, 1995, **268**, 1592–1595.

8 Z. Ge and S. Liu, *Macromol. Rapid Commun.*, 2009, **30**, 1523–1532.

9 E. Braun, Y. Eichen, U. Sivan and G. Ben-Yoseph, *Nature*, 1998, **391**, 775–778.

10 T. Scheibel, R. Parthasarathy, G. Sawicki, X.-M. Lin, H. Jaeger and S. L. Lindquist, *Proc. Natl. Acad. Sci. U. S. A.*, 2003, **100**, 4527–4532.

11 P. Broz, S. Driamov, J. Ziegler, N. Ben-Haim, S. Marsch, W. Meier and P. Hunziker, *Nano Lett.*, 2006, **6**, 2349–2353.

12 A. Blanazs, S. P. Armes and A. J. Ryan, *Macromol. Rapid Commun.*, 2009, **30**, 267–277.

13 A. Dehsorkhi, V. Castelletto, I. W. Hamley, J. Seitsonen and J. Ruokolainen, *Langmuir*, 2013, **29**, 14246–14253.

14 X. J. Loh, J. del Barrio, T.-C. Lee and O. A. Scherman, *Chem. Commun.*, 2014, **50**, 3033–3035.

15 P. P. Ghoroghchian, P. R. Frail, K. Susumu, D. Blessington, A. K. Brannan, F. S. Bates, B. Chance, D. A. Hammer and M. J. Therien, *Proc. Natl. Acad. Sci. U. S. A.*, 2005, **102**, 2922–2927.

16 R. Weissleder, *Science*, 2006, **312**, 1168–1171.

17 K. Cho, X. Wang, S. Nie, Z. Chen (Georgia) and D. M. Shin, *Clin. Cancer Res.*, 2008, **14**, 1310–1316.

18 H. Tanisaka, S. Kizaka-Kondoh, A. Makino, S. Tanaka, M. Hiraoka and S. Kimura, *Bioconjugate Chem.*, 2008, **19**, 109–117.

19 Q. Liu, H. Zhu, J. Qin, H. Dong and J. Du, *Biomacromolecules*, 2014, **15**, 1586–1592.

20 F. Ye, Å. Barrefelt, H. Asem, M. Abedi-Valugerdi, I. El-Serafi, M. Saghafian, K. Abu-Salah, S. Alrokayan, M. Muhammed and M. Hassan, *Biomaterials*, 2014, **35**, 3885–3894.

21 Y. Matsumura and H. Maeda, *Cancer Res.*, 1986, **46**, 6387–6392.

22 A. Makino, S. Kizaka-Kondoh, R. Yamahara, I. Hara, T. Kanzaki, E. Ozeki, M. Hiraoka and S. Kimura, *Biomaterials*, 2009, **30**, 5156–5160.

23 H. Cabral, Y. Matsumoto, K. Mizuno, Q. Chen, M. Murakami, M. Kimura, Y. Terada, M. R. Kano, K. Miyazono, M. Uesaka, N. Nishiyama and K. Kataoka, *Nat. Nanotechnol.*, 2011, **6**, 815–823.

24 K. Maruyama, *Adv. Drug Delivery Rev.*, 2011, **63**, 161–169.

25 J. C. Kraft, J. P. Freeling, Z. Wang and R. J. Y. Ho, *J. Pharm. Sci.*, 2014, **103**, 29–52.

26 Y. J. Jun, M. K. Park, V. B. Jadhav, J. H. Song, S. W. Chae, H. J. Lee, K. S. Park, B. Jeong, J. H. Choy and Y. S. Sohn, *J. Controlled Release*, 2010, **142**, 132–137.

27 M.-H. Lai, S. Lee, C. E. Smith, K. Kim and H. Kong, *ACS Appl. Mater. Interfaces*, 2014, **6**, 10821–10829.

28 D. Kokuryo, Y. Anraku, A. Kishimura, S. Tanaka, M. R. Kano, J. Kershaw, N. Nishiyama, T. Saga, I. Aoki and K. Kataoka, *J. Controlled Release*, 2013, **169**, 220–227.

29 J.-H. Fuhrhop and J. Mathieu, *J. Chem. Soc., Chem. Commun.*, 1983, 144–145.

30 J. H. Fuhrhop and D. Fritsch, *Acc. Chem. Res.*, 1986, **19**, 130–137.

31 Z. Xiao, M. Xu, M. Li, Z. Lu and Y. Wei, *Supramol. Sci.*, 1998, **5**, 619–622.

32 S. Pautot, B. J. Frisken and D. A. Weitz, *Proc. Natl. Acad. Sci. U. S. A.*, 2003, **100**, 10718–10721.

33 A. Uesaka, M. Ueda, T. Imai, J. Sugiyama and S. Kimura, *Langmuir*, 2014, **30**, 4273–4279.

34 M. Ueda, A. Makino, T. Imai, J. Sugiyama and S. Kimura, *Soft Matter*, 2011, **7**, 4143–4146.

35 M. Ueda, A. Makino, T. Imai, J. Sugiyama and S. Kimura, *Chem. Commun.*, 2011, **47**, 3204–3206.

36 E. Hara, A. Makino, K. Kurihara, F. Yamamoto, E. Ozeki and S. Kimura, *Int. Immunopharmacol.*, 2012, **14**, 261–266.

37 E. Hara, A. Makino, K. Kurihara, M. Sugai, A. Shimizu, I. Hara, E. Ozeki and S. Kimura, *Biochim. Biophys. Acta, Gen. Subj.*, 2013, **1830**, 4046–4052.

38 T. Ishida, M. Harada, X. Y. Wang, M. Ichihara, K. Irimura and H. Kiwada, *J. Controlled Release*, 2005, **105**, 305–317.

39 E. Hara, M. Ueda, C. J. Kim, A. Makino, I. Hara, E. Ozeki and S. Kimura, *J. Pept. Sci.*, 2014, **20**, 570–577.